2 MATERIALS AND METHODS

2.1 Chemicals

Analytical grade chemicals were used to conduct experiments. For safety reasons, non-radioactive isotope strontium nitrate ($Sr(NO_3)_2$) was used to prepare strontium solutions. It was purchased from Sigma Aldrich. Sulfuric acid (H_2SO_4, (98%)) was purchased from Loba Chemie and used for sulfuric acid leach reaction in the bentonite activation process. 1N HCl and HNO_3 were purchased from Loba Chemie and used to control solutions pH.

2.2 Adsorbent (SAB)

Bentonite samples were taken from Khulays area in the west of Saudi Arabia. The samples were received as large lumps. Crushing, sieving and drying processes were conducted to obtain the required particle size. Subsequently, samples were activated to increase its adsorption efficiency as Khulays natural bentonite has low activity [16]. As reported before [17], activation process was conducted by sulfuric acid leaching. This Activation process was investigated under different conditions of temperature, concentration of acid solution, degree and time of mixing and particle size of bentonite in order to find the best bentonite activity. In this study, activated samples of 200 mesh particle size were prepared by mixing with 15% sulfuric acid for 90 min at boiling temperature. The characterization of natural and SAB was realized using, BET, SEM, EDS, XRD, and FTIR. The spent SAB material can be reused after it undergoes reactivation process or can be disposed in a low-level radioactive waste landfill's sites. Reactivation of SAB will be conducted in the future work.

2.3 Adsorption process

Experiments were conducted in batches to investigate the adsorption of strontium ions from wastewater using SAB. Initially, 1000 mg/L of stock solution was prepared by strontium nitrate ($Sr(NO_3)_2$) addition in distilled water. Different strontium concentrations were prepared as required by adding distilled water in order to reduce the concentration of stock solution. 50 ml of solution is added in each batch of flasks and shacked horizontally in water bath (Model. JULABO SW 22). Flasks were shaken at 200 rpm at room temperature for a certain time then removed from the shaker. The mixture in each flask was separated using centrifugal device (Model: ROTOFIX 32A) working at 4000 rpm for 15 min. The separated supernatant was measured for strontium concentration using atomic absorption spectrophotometer. The adsorption percentage was measured as:

$$Ads\ \% = \frac{C_i - C_t}{C_i}, \tag{1}$$

where C_i (mg L^{-1}) and C_t (mg L^{-1}) are the initial and final time concentration, respectively. The amount of strontium adsorbed at equilibrium given as:

$$q_e = \frac{(C_i - C_e)V}{m}, \tag{2}$$

where, C_e presents equilibrium concentration of strontium (mg L^{-1}), V is the solution volume (L) and m being SAB mass (g).

3 RESULT AND DISCUSSION

3.1 Adsorbent characterization

N_2-BET was used to find the natural and activated bentonite (SAB) surface area. The measured surface area of natural bentonite was 64.2 m^2/g and increased to 303 m^2/g after sulfuric acid treatment. The SEM images of the natural and H_2SO_4 activated bentonite are shown in Fig. 1. A Quanta Scanning Electron Microscopy with field emission gun (FEG) systems containing an Everhart Thornley detector (ETD) and a solid-state back scattering electron detector (VCD) for bright-field and dark-field sample imaging. A densely packed structure was observed for natural bentonite compared to the activated bentonite, may be a cause of leaching out some of the materials during activation process also the EDS analysis suggests an increase in Si atom% in activated bentonite (26.37 atom%) compared to natural bentonite (21.48 atom%) which may bring us to the conclusion of increment of the quartz (SiO_2) phase in the activated bentonite and later on we also observed the same for IR and XRD analysis of the samples. From EDS analysis, elemental composition of the bentonite samples was identified which are comprised of mainly oxygen and silicon (which makes the quartz structure) and tress amount alumina, iron, copper, potassium, sulphur, sodium, magnesium.

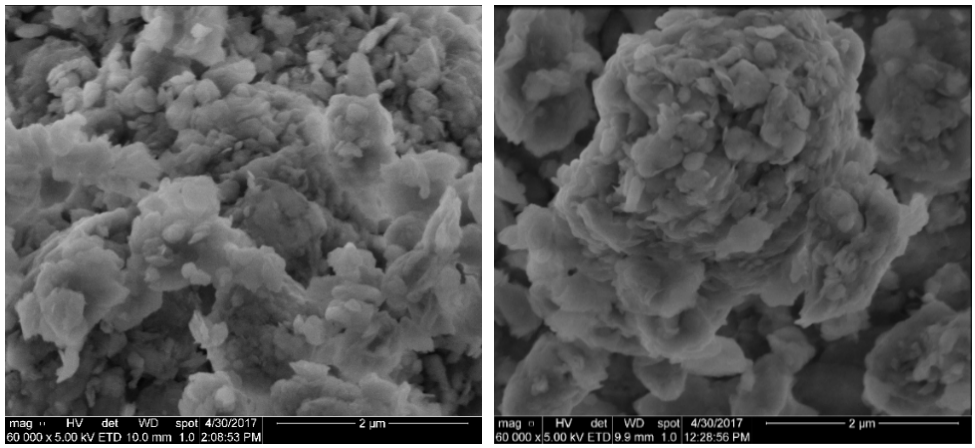

(a) (b)

Figure 1: SEM image for: (a) Natural bentonite; and (b) Activated bentonite (SAB).

An IR study was conducted for the sample using Bruker Tensor II FTIR spectrometer (closed system). The IR spectra of natural and H_2SO_4 activated bentonite can be seen in Fig. 2. The strong adsorption band around 1000 cm^{-1} (1021 cm^{-1} for natural bentonite and 1044 cm^{-1} for activated bentonite) relates to the Quartz Si-O bending vibration. The adsorption band around 1591 cm^{-1} and 3306 cm^{-1} is for H_2O (hydroxyls bound via H bond) and small peak at 3644 cm^{-1} is for stretching frequency of structural OH group. No significant change in the IR peaks/bands are observed. Except broadening of the Si-O band at around 1044 cm^{-1}. The peak broadening may be due to the changes made to the quartz structure during activation process with H_2SO_4. The change may be in the change of phase orientation and that is also observed in XRD analysis.

The diffraction of the prepared SAB was measured using Equinox 1000 bench top X-Ray Diffractometer with CPS 180 detector using cobalt Kα1 radiation. Match© Crystal Impact software was used to identify phases (using both COD and ICSD databases). The XRD analysis of the samples (natural and H_2SO_4 activated) are depicted in the Fig. 3. The XRD analysis confirmed a bentonite structure composed of Quartz-SiO_2 phase and montmorillonite phase as it has been reported in many previous studies. In a close observation between the two bentonite samples, there is no change in peak position except in some places an increase in peak intensity is observed, especially at 2^{θ}=26.6° the change in peak intensity can be clearly identified. This peak belongs to (210) plane of quartz-SiO_2. So, the activation process makes the bentonite planes more oriented in Quartz (210) plane. Also, there are some minute changes in montmorillonite phases in the range (2^{θ}=20–25°) but not significant. The increase in Quartz phase was also observed in IR spectrometric analysis.

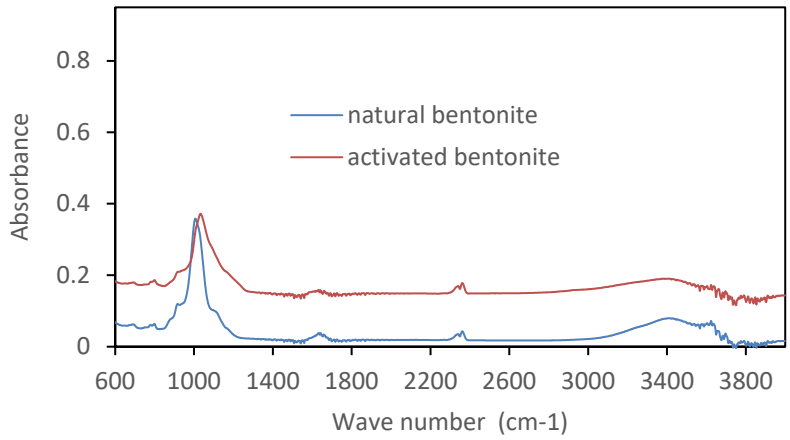

Figure 2: FTIR analysis for natural bentonite and SAB.

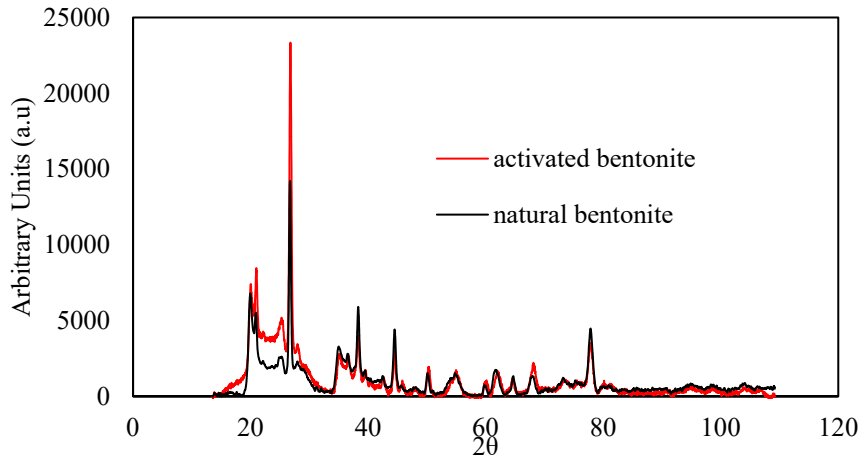

Figure 3: XRD analysis for natural and activated bentonite (SAB).

3.2 Effect of mixing time

The adsorption percentage was evaluated at a time varying between 5 to 120 min. Shaking strontium solution with certain amount of SAB (0.25 g) was investigated for determining the equilibrium adsorption time. The adsorption process tests were conducted on series of batches, each of which had strontium concentration varying between 10 and 100 mg/L. The mixture pH in each flask was measured during the experiment without any change at 3.4. Lower pH of the mixture was due to the concentrated sulfuric acid used in bentonite activation process. The shaking speed was 200 rpm at room temperature (25°C). Presented in Fig. 4 strontium adsorption on SAB was rapid in the beginning of each experiment with a sharp increase in the adsorption percentage during the first 10 minutes. Afterwards, a gradual increase was observed before the adsorption process reached equilibrium after 50 minutes. This time is quite less compared to other adsorbents as reported [8], [18]. Moreover, the adsorption percentage was decreased from 85%–30% as the initial strontium solution increased from 10–100 mg/L. This is due to the decreased in the available sites on the adsorbent surface, occupied by strontium ions present in the solution. Therefore, mixing strontium solution with SAB for 50 min is enough to attain equilibrium and in all subsequent experiments solution is treated with bentonite for 50 min to ensure equilibrium adsorption.

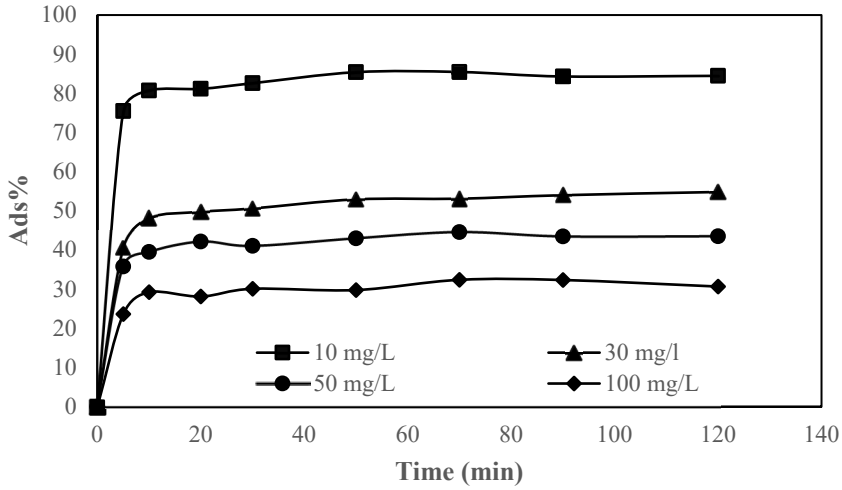

Figure 4: Effect of mixing time (min).

3.3 Effect of pH

Solution pH is an important factor controlling heavy metals adsorption dissolved in water. Adsorption of strontium ions onto SAB was tested at different solution pH ranging from 1–10. Initial strontium concentration is maintained at 50 mg/L with bentonite ratio of 0.25 g/50 ml strontium solution at room temperature (25°C). The solution was shaken for 50 min to reach equilibrium while the pH was adjusted during the experiments using 1N HCl and 1N HNO_3. Fig. 5 shows week strontium adsorption percentage when the solution pH varies between 1 and 4. Adsorption percentage was increased rapidly when solution pH increased to 5 till 7. Any further increase in pH does not offer substantial adsorption. In acidic medium (pH < 4), low adsorption percentage was observed as a result of positive charge increase on

SAB surface. Strontium ions and SAB surface repel each other due to electrostatic positive charge on their surfaces [19], [20]. Furthermore, lower pH means high hydrogen ions (H+) concentration, which compete with strontium ions in the solution and thus, decreases strontium ions adsorption efficiency. At (4 < pH < 7), adsorption percentage increases due to the decrease in electrostatic repulsion as well as lesser H+ ions resulting in strontium adsorption increase. The increase in adsorption with increasing solution pH above 7 may be attributed to precipitation of $Sr(OH)_2$ rather than adsorption [21]. Subsequent, experiments are conducted using solution pH at 7.

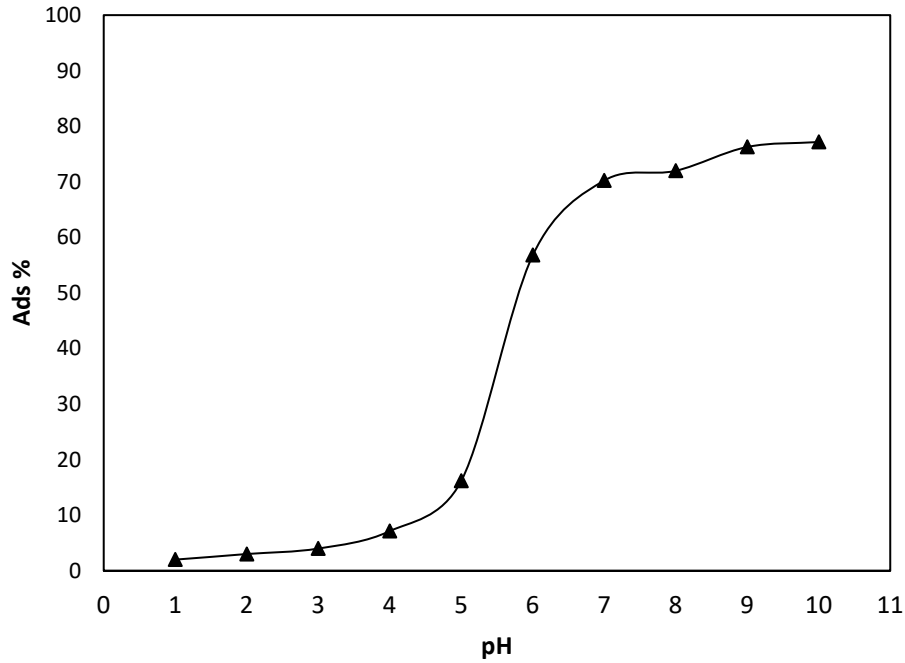

Figure 5: Effect of pH.

3.4 Sr initial concentration effects

The adsorption process was investigated by varying the initial strontium ions mass from 8 to 115 mg/L. The other parameters were held constant including solution pH at 7, mass of adsorbent ratio at 0.25g/50 ml strontium solution at ambient temperature (25°C). Fig. 6(a) presents the adsorption percentage of strontium versus the initial strontium concentration. It shows higher adsorption at lowest initial strontium concentration (8 mg/L) and decreased gradually with increasing initial strontium concentration and reaches 40% at concentration of 115 mg/L. This behaviour may be attributed to the saturation of exchangeable active sites on adsorbent surface by strontium ions which increases with high strontium ions concentration. Rapid adsorption and higher adsorption at low strontium concentration makes SAB an adsorbent having high capacity to remove strontium ions from wastewater.

3.5 SAB concentration effects

Bentonite concentration for adsorption process is tested by varying the mass of SAB from 0.03 to 1.5g/50 ml of strontium solution. All the other parameters were kept constant, i.e. 50 mg/L of strontium, 50 min of shaking (equilibrium time) and solution pH of 7 at room temperature (25°C). Fig. 6(b) displays the relation between the adsorption percentage and SAB dosage. The plot trend shows rapid increase of the adsorption percentage with increasing of SAB dosage when SAB dosage was between 0.03 and 0.75 g. it is clear that 0.75g of SAB was sufficient to remove all of strontium ions in the solution. Further addition of bentonite is futile. Increase in active sites to adsorb strontium ions may have resulted in such behaviour as adsorbent dosage is increased [22].

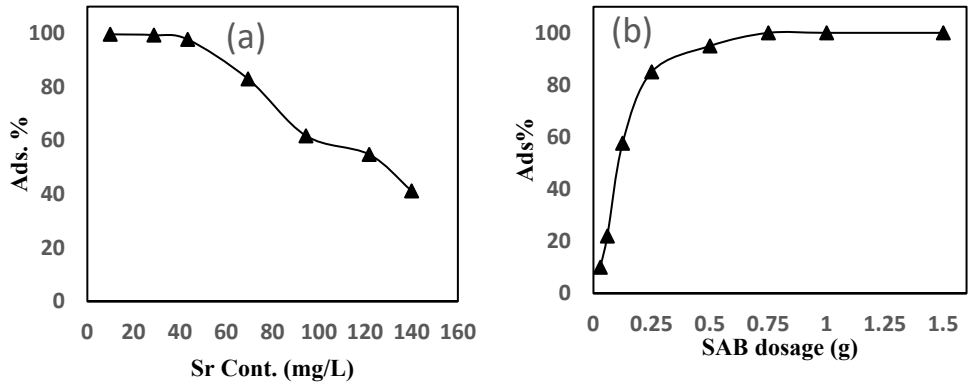

Figure 6: Effect of: (a) Sr concentration; and (b) SAB dosage.

3.6 Adsorption isotherm

Study of adsorption isotherm is important for system design purposes. Furthermore, it can be used to understand how adsorbed ions interact with the adsorbent surfaces and the adsorption mechanism. The adsorption isotherms were studied with different initial strontium ions concentration ranging from 8–115 mg. 0.25 g of bentonite was added to 50 ml of strontium solution. Time and solution pH were adjusted to 50 min and 7, respectively. Adsorption of strontium ions onto SAB data may follow Langmuir or Freundlich models. Former assumes single layer adsorption onto adsorbent surfaces while the interaction between the adsorbed particles is ignored. The Langmuir eqn is written in the form [23]:

$$\frac{C_e}{q_e} = \frac{1}{bQ_{\max}} + \frac{C_e}{Q_{\max}}, \tag{3}$$

where Q_{max} is the maximum adsorption capacity of SAB (mg g^{-1}) while b is termed as model constant (L mg^{-1})

Adsorption non-linear surfaces are usually characterized by using Freundlich isotherm eqn which can be written as [24]:

$$logq_e = logkK_F + \frac{1}{n} logC_e \tag{4}$$

K_F and n presents the model constants. It is clear from Fig. 7 that the experimental data for strontium adsorption on SAB was well fitted to Langmuir and Freundlich models with linearized regression coefficient (R^2) 0.993 and 0.834, respectively. However, data fitting is better for Langmuir than Freundlich. The maximum sorption capacity, Q_{max} of SAB was calculated as shown in Table 1 as 11.98 mg/g. Furthermore, Freundlich model parameters were also evaluated. The values of constant n=5.0 reveals a strong adsorption capacity as its value is in between 0 and 10 [12], [25].

Table 1: Isotherm models parameters.

Model	Isotherm constants		
Langmuir	Q_{max} (mg g^{-1})	b (L mg^{-1})	R^2
	11.98	29.8	0.993
Freundlich	K_F (mg g^{-1})	n	R^2
	6.09	5.0	0.834

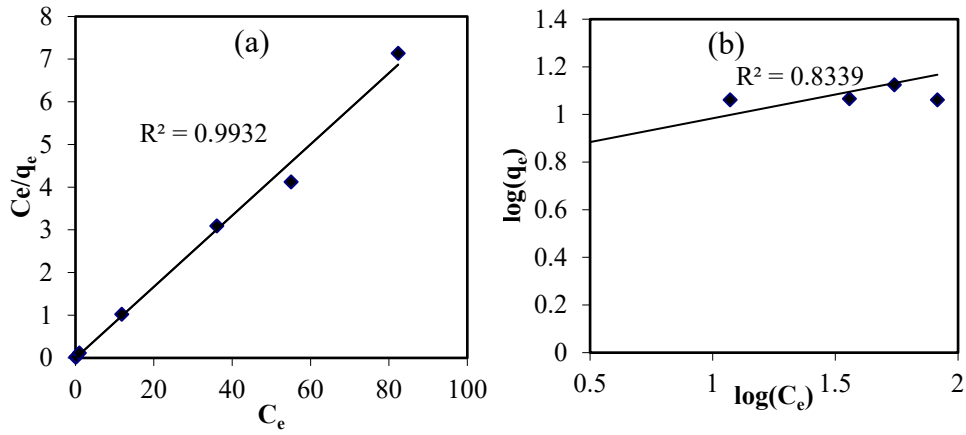

Figure 7: Isotherm models: (a) Langmuir model; and (b) Freundlich model.

3.7 Adsorption kinetic

Sorption kinetic experiments were conducted in a batch mode using strontium solution of 10,30,50 and 100 mg/L. The other parameters were constant at bentonite dosage ratio of 0.25 g/ 50 ml of strontium solution, pH at 3.4 and at room temperature (25°C). Pseudo-first order and second kinetic models were fitted to experimental data. The pseudo-first order is represented by Lagergren [26] eqn as follows:

$$\log(q_e - q_t) = log q_e - \frac{K_1}{2.303} t. \quad (5)$$

The following eqn provides a linearized relation of pseudo-second order model:

$$\frac{t}{q_t} = \frac{1}{K_2 q_e^2} + \frac{1}{q_e} t, \quad (6)$$

where K_1 (min^{-1}) and K_2 (g mg^{-1} min^{-1}) represents the model parameters for pseudo-first and second order kinetic model, respectively. The results as shown in Table 2. Fig. 8 shows a good agreement between the experimental data and the pseudo-second order. The correlation factor (R^2) is very close to 1 for all initial strontium concentration (10–100 mg/L) comparing to low value for pseudo first order ($R > 0.6$). It means that the chemisorption mechanism is controlling the adsorption of strontium onto SAB [13], [22]. The values of rate constant K_2 and q_e were calculated from the slope and the intercept of the straight lines. A decrease in K_2 value is observed (Table 2) for increasing strontium initial concentration. Furthermore, equilibrium adsorption of strontium (q_e) also increases when initial strontium concentration increases. This may be attributed to the higher available adsorbent sites available to adsorb strontium ions at low initial strontium concentration.

Table 2: Kinetic parameters for pseudo-second model.

C_o (mgL^{-1})	T (K)	K_2 (g mg^{-1} min^{-1})	q_e (mg g^{-1})	R^2
10	298	1.4	1.70	0.9999
30	298	0.2	3.3	0.9995
50	298	0.18	4.28	0.9998
100	298	0.15	6.60	0.998

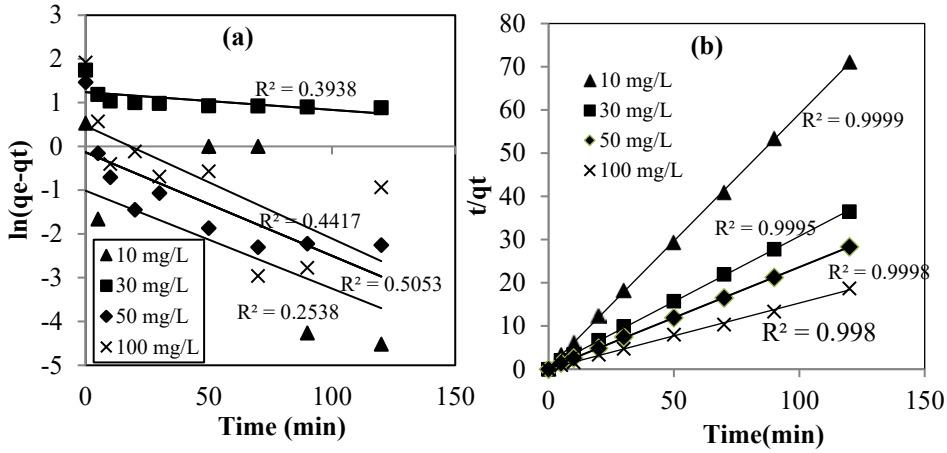

Figure 8: Adsorption kinetic models: (a) Pseudo-first order; and (b) Pseudo-second order.

3.8 Thermodynamic study

Temperature may affect the strontium adsorption by porous SAB. 0.25 g of SAB is added in 50 ml of strontium solution giving resultant concentration of 50 mg/L. The mixture was mixed for 50 min to ensure the equilibrium was achieved. The same experiment was repeated while the solution temperature was controlled at 298, 308 and 318K. To explore the mechanism of adsorption of strontium on SAB, adsorption system energy parameters including Gibbs free energy of adsorption (ΔG^o), Enthalpy change of adsorption (ΔH^o) and Entropy change of adsorption (ΔS^o) were determined using the following eqns:

$$\Delta G^o = -RT \times \ln (K_D), \tag{7}$$

$$\ln(K_D) = \frac{\Delta S^o}{R} - \frac{\Delta H^o}{RT}, \tag{8}$$

where T is the absolute temperature in Kelvin, R is the gas constant (8.314×10^{-3}), and K_D ($= q_e/C_e$) is known as the distribution coefficient.

Relation between K_D and 1/T is shown in Fig. 9, where ΔH^o and ΔS^o being the slope and the intercept of the plot, respectively. Thermodynamic parameters for the adsorption process are shown in Table 3 at three different temperatures, 298, 308 and 318 K. Spontaneous rates are elucidated by the negative values of free energy (ΔG^o). As the values of enthalpy (ΔH^o) and entropy (ΔS^o) are positive with values of 40.4 kJ mol^{-1} and 52.78 J mol^{-1} K^{-1} respectively, suggests endothermic as well as rapid adsorption process. Similar studies are conducted with corresponding results for the removal of various heavy metals [27], [28]. Furthermore, change in pore size may be attributed to increased temperatures which increases adsorption capacity of SAB. Temperature also increases the rate of interparticle diffusion of strontium ions [29].

Table 3: Strontium adsorption thermodynamic data onto SAB.

Temperature (°C)	ΔG (kJ mol^{-1})	ΔH (kJ mol^{-1})	ΔS (J mol^{-1} K^{-1})
298	-2.71		
308	-3.54	20.4	52.78
318	-4.26		

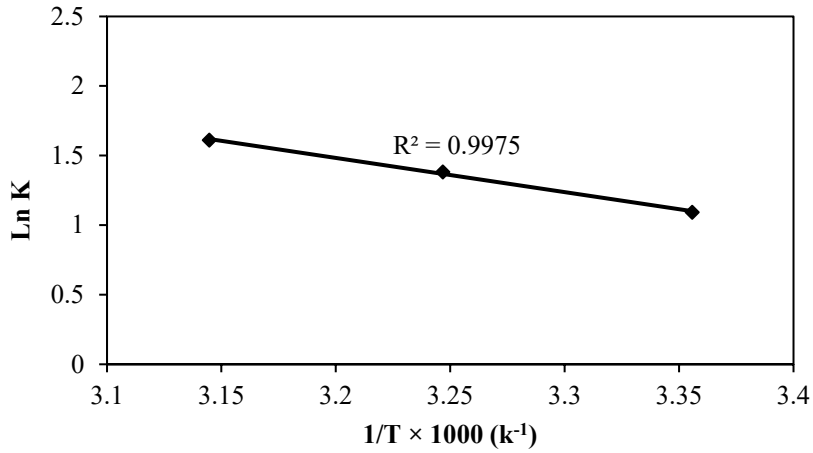

Figure 9: Plot of ln K versus $1/T$ for adsorption of strontium on SAB.

4 CONCLUSION

Adsorption of strontium on SAB was investigated at different experimental conditions. Adsorption of strontium on SAB was rapid and it takes 50 min to reach equilibrium adsorption. The process was pH dependent where increasing the solution pH increased the adsorption percentage. In acidic medium, lower pH (pH <4) means high hydrogen ions (H^+) concentration, which competes with strontium ions in the solution and thus, decreases

strontium ions adsorption efficiency. At (4 < pH < 7), adsorption percentage increases due to lesser H^+ ions resulting in strontium adsorption increase. The increase in adsorption with increasing solution pH above 7 may be attributed to precipitation of $Sr(OH)_2$ rather than adsorption. The adsorption percentage decreased with increasing of initial strontium concentration. Furthermore, increasing SAB dosage increased the adsorption percentage because of increase in active sites. Data can be fitted by Langmuir as well as Freundlich adsorption models but isotherm fit better to Langmuir than Freundlich. The maximum loading capacity of SAB was 11.98 mg/g. The process is chemisorption in nature as experimental data was modelled with pseudo-second order equation. Thermodynamic study of strontium on SAB confirms spontaneous and endothermic process. In the future work, efficiency of the adsorption process using SAB needs to be investigated in the presence of other ions in wastewater such caesium and other cations (K^+, Na^+, Ca^{2+} and Mg^{2+}).

REFERENCES

[1] Salbu, B. et al., Radioactive contamination from dumped nuclear waste in the Kara Sea – results from the joint Russian-Norwegian expedition in 1992–1994. *The Science of the Total Environment*, **202**, pp. 185–198, 1997.

[2] Matsunaga, T. et al., Characteristics of Chernobyl-derived radionuclides in particulate form in surface waters in the exclusion zone around the Chernobyl Nuclear Power plant. *Journal of Contaminant Hydrology*, **35**, pp. 101–113, 1998.

[3] Galamboš, M., Kufčáková, J., Rosskopfová, O. & Rajec, P., Adsorption of cesium and strontium on natrified bentonites. *Journal of Radioanalytical and Nuclear Chemistry*, **283**, pp. 803–813, 2010.

[4] USEPA, *Implementation Guidance for Radionuclides: Implementation Guidance for Radionuclides; EPA-816-F-00-002*. Office of Ground Water and Drinking Water: USEPA, Washington, DC, 2002.

[5] Chen, X., Peng, S.C. & Wang, J., Retention profile and kinetics characteristics of the radionuclide 90-Sr(II) onto kaolinite. *Journal of Radioanalytical and Nuclear Chemistry*, **303**, pp. 509–519, 2015.

[6] Erten, H.N., Aksoyoglu, S., Hatipoglu, S. & Gokturk, H., Sorption of cesium and strontium on montmorillonite and kaolinite. *Radiochimica Acta*, **44/45**, pp. 147–151, 1988.

[7] Reinoso-Maset, E. & Ly, J., Study of major ions sorption equilibria to characterize the ion exchange properties of kaolinite. *Journal of Chemical & Engineering Data*, **59**, pp. 4000–4009, 2014.

[8] Al Attar, L., Safia, B. & Abdul Ghani, B., Uptake of 137Cs and 85Sr onto thermally treated forms of bentonite. *Journal of Environmental Radioactivity*, **193–194**, pp. 36–43, 2018.

[9] Galamboš, M., Krajnak, A., Rosskopfová, O., Viglasova, E., Adamcova, R. & Rajec, P., Adsorption equilibrium and kinetic studies of strontium on Mg-bentonite, Fe-bentonite and illite/smectite. *Journal of Radioanalytical and Nuclear Chemistry*, **298**, pp. 1031–1040, 2013.

[10] Missana, T. & Garcı´a-Gutie´rrez, M., Adsorption of bivalent ions (Ca(II), Sr(II) and Co(II)) onto FEBEX bentonite. *Physics and Chemistry of the Earth*, **32**, pp. 559–567, 2007.

[11] Möller T., Harjula, R. & Paajanen, A., Removal of 85Sr, 134Cs, and 57Co radionuclides from acidic and neutral waste solutions by metal doped antimony silicates. *Separation Science and Technology*, **38**(12–13), pp. 2995–3007, 2007.

[12] Zhang, L., Wei, J., Zhao, X., Li, F. & Jiang, F., Adsorption characteristics of strontium on synthesized antimony silicate. *Chemical Engineering Journal*, **277**, pp. 378–387, 2015.
[13] Al-Shahrani, S.S., Treatment of wastewater contaminated with cobalt using Saudi activated bentonite. *Alexandria Engineering Journal*, **53**, pp. 205–211, 2014.
[14] Al-Shahrani, S.S., Treatment of wastewater contaminated with Fe(II) by adsorption onto Saudi activated bentonite. *International Journal of Engineering & Technology*, **13**(6), pp. 62–72, 2013.
[15] Al-Shahrani, S.S., Removal of cadmium from wastewater using Saudi activated bentonite. *WIT Transactions on Ecology and The Environment*, vol. 163, pp. 391–402, 2012.
[16] Al-Shahrani, S., Removal of lead from aqueous solutions using Saudi activated Bentonite. *WIT Transactions on Ecology and the Environment*, **135**, pp. 277–288, 2010.
[17] Al-Shahrani, S., The feasibility of producing active clay from a local raw material by sulfuric acid leaching. M.Sc thesis, King Abdulaziz University, 1998.
[18] Başçetina, E. & Atun, G., Adsorption behavior of strontium on binary mineral mixtures of Montmorillonite and Kaolinite. *Applied Radiation and Isotopes,* **64**, pp. 957–964, 2006.
[19] Sarı, A., Tuzen, M. & Soylak, M., Adsorption of Pb(II) and Cr(III) from aqueous solution on Celtek clay. *Journal of Hazardous Materials*, **B144**, pp. 41–46, 2007.
[20] Ghaemi, A., Torab-Mostaedi, M. & Ghannadi-Maragheh, M., Characterizations of strontium(II) and barium(II) adsorption from aqueous solutions using dolomite powder. *Journal of Hazardous Materials*, **190**, pp. 916–921, 2011.
[21] Liang, T.-J., Hsu, C.-N. & Liou, D.-C., Modified freundlich sorption of cesium and strontium on Wyoming bentonite. *Applied Radiation and isotope*, **44**(9), pp. 1205–1208, 1993.
[22] Huang, F., Yi, F., Wang, Z. & Li, H., Sorptive removal of Ce(IV) from aqueous solution by bentonite. *Procedia Environmental Sciences*, **31**, pp. 408–417, 2016.
[23] Langmuir, I., The adsorption of gases on plane surfaces of glass, mica and platinum. *Journal of the American Chemical Society*, **40**, pp. 1361–1403, 1918.
[24] Freundlich, H.M.F., Uber die Adsorption in Losungen. *Zeitschrift für Physikalische Chemie*, **57**, pp. 385–470, 1906.
[25] Shikuku, V.O., Donato, F.F., Kowenj, C.O., Zanella, E.R. & Prestes, O.D., A comparison of adsorption equilibrium, kinetics and thermodynamics of aqueous phase clomazone between faujasite X and a natural zeolite from Kenya. *South African Journal of Chemistry*, **68**, pp. 245–252, 2015.
[26] Lagergren, S., Zur theorie der sogenannten adsorption gelöster stoffe. *Kungliga Svenska Vetenskapsakademiens*, *Handlingar*, **24**(4), pp. 1–39, 1898.
[27] Sharma, Y.C., Uma Srivastava, V., Srivastava, J. & Mahto, M., Reclamation of Cr(VI) rich water and wastewater by wollastonite. *Chemical Engineering Journal,* **127**, pp. 151–156, 2007.
[28] Elouear, Z., Bouzid, J., Boujelben, N., Feki, M., Jamoussi, F. & Montiel, A., Heavy metal removal from aqueous solutions by activated phosphate rock. *Journal of Hazardous Materials*, **156**(1–3), pp. 412–420, 2008.
[29] Nityanandi, D. & Subbhuraam, C.V., Kinetics and thermodynamic of adsorption of chromium(VI) from aqueous solution using puresorbe. *Journal of Hazardous Materials*, **170**, pp. 876–882, 2009.